Lithuanian Journal of Physics, Vol. **48**, No. 1, pp. 79–84 (2008) doi:10.3952/lithjphys.48106

CHARACTERIZATION OF SiC CRYSTALS BY OPTICAL AND ELECTRICAL MEANS

K. Neimontas, R. Vasiliauskas, A. Mekys, J. Storasta, and K. Jarašiūnas

Institute of Materials Science and Applied Research, Vilnius University, Saulėtekio 9, LT-10222 Vilnius, Lithuania
E-mail: kestutis.jarasiunas@ff.vu.lt

Received 22 October 2007; revised 15 November 2007; accepted 21 November 2007

Measurements of carrier transport have been carried out in different SiC polytypes by using two complementary techniques: a picosecond four-wave mixing and magnetoresistance. Both techniques confirmed the mechanism of phonon scattering in $T =$ 100–300 K range, as well as higher carrier mobility in n-type 4H epitaxial layers with respect to 3C-SiC. The optical technique revealed a decrease of the bipolar mobility in 3C-SiC at $T < 100$ K and its variation with photoexcited carrier density. A lattice heating was observed in free standing 3C- and 4H-SiC due to strong impact of nonradiative recombination, and this effect precluded optical studies of carrier dynamics at low temperatures.

Keywords: silicon carbide, carrier transport, lattice heating, transient gratings

PACS: 72.20.Jv, 78.47.+p

1. Introduction

Devices made from SiC have been under extensive development in the past two decades and some of them are already commercialized. They often operate at high carrier densities, therefore it is important to determine carrier plasma parameters under adequate conditions. Non-destructive monitoring of carrier plasma parameters at high injection conditions is possible by using "excite-probe" optical techniques, which explore the light-induced changes of absorption or refractive index by free carriers [1, 2]. Transient grating, or four-wave mixing technique (FWM) may provide all-optical evaluation of carrier transport and recombination processes in a wide range of excitations. Moreover, optical carrier injection at different wavelengths with quantum energies above the bandgap makes it possible to vary in-depth resolution, to reach high nonequilibrium carrier density, and to study carrier density dependent photoelectric processes [3].

In this work, we applied the optical and electrical techniques to study carrier dynamics and transport in differently grown 4H-SiC and 3C-SiC samples in 10–300 K range. By optical technique, we determined the temperature dependence of the bipolar carrier mobility in wide range of excitations. Comparative electrical measurements in 100–300 K range confirmed the dominant phonon scattering mechanism in the given temperature range. At lower temperatures ($T < 100$ K), a decrease of bipolar mobility in 3C-SiC reflected the ionized impurity scattering, while the screening of local charge by higher nonequilibrium carrier density resulted in higher mobility values. Moreover, at temperatures below 100 K, we observed strong contribution of a lattice heating to refractive index modulation, and this effect precluded optical studies of carrier dynamics at temperatures below 100 K in the samples with high defect density.

2. Samples

We performed measurements of nonequilibrium carrier dynamics in n-type 3C-SiC (111) epilayer grown by vapour–liquid–solid (VLS) mechanism on 6H-SiC (0001) and carried out comparative studies on free-standing bulk 3C-SiC (001) material originally grown on Si by HOYA Co. The 5 μm thick n-type ($n_0 \approx 10^{17}$ cm^{-3}) 3C-SiC (111) epilayer was elaborated in two steps: firstly, a 2 μm double-positioning boundary (DBP) free layer was grown by VLS mechanism in Ge-Si melt as described in Ref. [4]. After wet etching of the sample in acid solution to remove the remaining Ge-Si alloy on the surface, the 3C-SiC layer was thickened to 5 μm by standard chemical vapour deposition (CVD) growth at 1450 °C using a mixture of silane and propane diluted in H_2.

ISSN 1648-8504

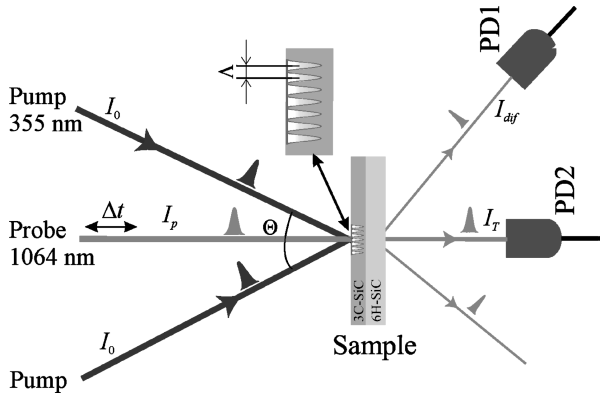

Fig. 1. Optical configuration for a surface grating recording. I_0, I_p, I_dif, and I_T are the intensities of pump, probe, diffracted, and transmitted beams, correspondingly, Λ is the period of diffraction pattern, Θ is the angle between pump beams.

The measurements were also performed on two differently grown n-type 4H-SiC epilayers. One of them was 35 μm thick layer ($n_0 = 10^{16}$ cm^{-3}) grown by CVD on a heavily doped ($n_0 = 10^{19}$ cm^{-3}) 4H-SiC substrate. The second one was 30 μm thick layer ($n_0 = 5{\cdot}10^{15}$ cm^{-3}) grown by sublimation technique on a semi-insulating 4H-SiC substrate.

3. Experimental technique

The samples were excited by the interference pattern of two 25 ps duration laser beams at 355 nm wavelength, which created a periodically modulated nonequilibrium carrier density $N(x) = N_0 + \Delta N \times \cos(2\pi x/\Lambda)$ with the period Λ and refractive index modulation by free carriers $\Delta n_\mathrm{FC}(x,t) \sim \Delta N(x,t)$ [2]. The incident light was absorbed in a layer of thickness $d = \alpha^{-1} \sim 48$ μm (in 4H-SiC) or $d \sim 4.5$ μm (in 3C-SiC sample), in accordance with the absorption coefficient α, thus creating the nonequilibrium ambipolar carrier plasma of density up to 10^{18} cm^{-3}. A delayed probe pulse at 1064 nm, to which SiC samples were transparent, monitored the instantaneous diffraction efficiency (Fig. 1) of the grating $\eta = I_\mathrm{dif}/I_\mathrm{T}$ (here I_dif is the diffracted and I_T is the transmitted probe beam intensity), which is proportional to the square of refractive index modulation, i. e. $\eta(t) \sim \Delta n^2_\mathrm{FC}(t) = (n_\mathrm{eh}\,\Delta N)^2$ (n_eh is refractive index change induced by one electron–hole pair) [2]. The carrier grating decay time τ_G is obtained by an exponential fit of diffraction efficiency decay kinetics $\eta \sim \exp(-2t/\tau_\mathrm{G})$. The grating is erased by carrier recombination and lateral diffusion processes, therefore τ_G can be expressed through ambipolar diffusion coefficient D_a and carrier recombination time τ_R [2]:

$$\frac{1}{\tau_\mathrm{G}} = \frac{1}{\tau_\mathrm{R}} + \frac{4\pi^2 D_\mathrm{a}}{\Lambda^2}\,. \tag{1}$$

The decay of free-carrier grating with carrier density $N(x,t)$ is described by

$$\frac{\partial N(x,t)}{\partial t} = D_\mathrm{a}(N)\frac{\partial^2 N(x,t)}{\partial x^2} - \frac{N(x,t)}{\tau_\mathrm{R}} \tag{2}$$

$$- B\,N^2(x,t) - C\,N^3(x,t) + G(x,t)\,.$$

Here C is the Auger recombination coefficient, B is the bimolecular recombination coefficient, and $G(x,t) = \alpha\,I(x,t)/(h\nu)$ is the carrier generation function.

For the measurements of magnetoresistance, the samples were made as classic Hall bar-shape pieces ($2{\times}5{\times}0.4$ mm^3) with planar indium contacts. Samples were placed in a nitrogen-cooled cryostat with magnetic field $B = 1.75$ T. Current was controlled with a KEITHLEY 6430 multimeter. The measurements were performed in 100–400 K temperature range.

From magnetoresistivity measurements, the magnetoresistant mobility of equilibrium carriers can be calculated [5]:

$$\mu_\mathrm{M} = \frac{r_\mathrm{M}}{B}\sqrt{\frac{\rho_B - \rho_0}{\rho_0}}\,, \tag{3}$$

here B is applied magnetic field, ρ_B is magnetoresistivity, ρ_0 is resistivity, r_M is a constant which depends on sample geometry and scattering mechanisms. The magnetoresistant mobility is mainly influenced by the largest current. Therefore, for n-type samples with mobility of electrons being higher than that of holes ($\mu_\mathrm{h} \ll \mu_\mathrm{n}$), the magnetoresistant mobility reflects the electron mobility. Carrier scattering mechanisms can be identified from the index value of the temperature dependence of magnetoresistant mobility: if phonon scattering dominates, then $\mu_\mathrm{M} \sim T^{-3/2}$, if ionized impurities – $\mu_\mathrm{M} \sim T^{3/2}$, if dislocations – $\mu_\mathrm{M} \sim T$ [6].

4. Results and discussion

We measured grating decay kinetics at different grating periods Λ (in range from 2.7 to 14 μm), excitation intensities, and temperatures (10–300 K). Using a set of the measured grating kinetics at various periods and the corresponding grating decay times τ_G, we determined the bipolar diffusion coefficients D_a and carrier lifetimes by using Eq. (1). The bipolar mobility values μ_a were obtained from the Einstein relation

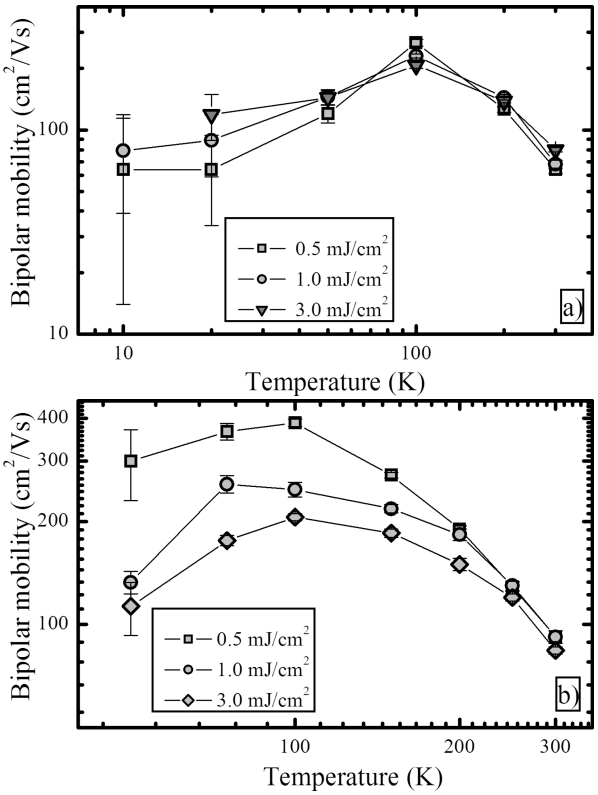

Fig. 2. Temperature dependence of a bipolar mobility in (a) 3C-SiC (111) epitaxial layer and (b) free standing 3C-SiC (001) substrate at different excitation energy densities.

$D_{\rm a} = (kT/e)\mu_{\rm a}$. Under our experimental conditions, the electron and hole concentrations are equal ($\Delta N_{\rm e} \approx \Delta N_{\rm h}$), thus the hole mobility ($\mu_{\rm h} \ll \mu_{\rm n}$) limits the value of bipolar diffusion coefficient $D_{\rm a} \approx 2D_{\rm h} = 2kT\mu_{\rm h}/e$. The hole mobility in free standing 3C-SiC layer at 300 K was found to be equal to $\mu_{\rm h} = (40\pm5)$ cm^2/(V s), and a slightly smaller value of $\mu_{\rm h} = (35\pm5)$ cm^2/(V s) was found in epitaxial DPB free layer. The decrease of bipolar mobility (see Fig. 2(a, b)) at low temperatures ($T < 100$ K) reflected the ionized impurity scattering, while at higher temperatures ($T > 100$ K) the phonon scattering dominated. In the conditions of ionized impurity scattering, we found a tendency of mobility increase with increasing excitation density for the epitaxial 3C-SiC layer, while in the free standing 3C-SiC layer the effect was opposite: the μ value decreased from 300 to 110 cm^2/(V s) at $T = 50$ K, see Fig. 2(b). These tendencies can be attributed to screening of the charge at contributing defect states by high carrier density. Carrier mobility values were found to be higher in the free standing layer in all measured temperature range, and that shows better electrical properties of the sample in comparison with the DPB free epilayer. In the latter sample, photoluminescence measurements revealed high density of shallow impurities (above 10^{18} cm^{-3})

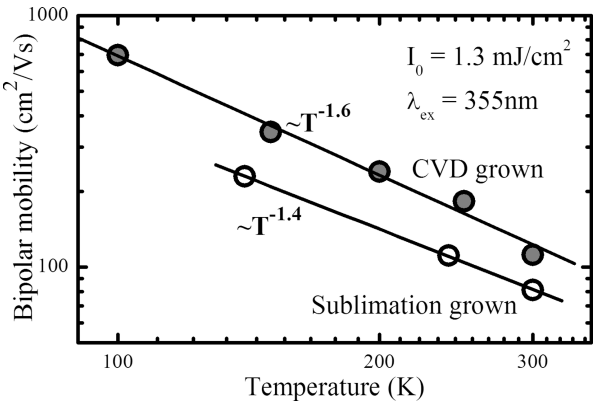

Fig. 3. Temperature dependence of bipolar carrier mobility in differently grown n-type 4H-SiC epilayers.

[7], while in the bulk 3C-SiC the concentration of nitrogen donors was in mid-10^{15} cm^{-3} [8].

In Fig. 3 we show the decrease of bipolar mobility with temperature at two different 4H-SiC epilayers at $I_0 = 1.3$ mJ/cm^2 excitation intensity. The measured temperature dependence $\mu_{\rm a} \sim T^{-A}$ was found to be similar to those typical for phonon (lattice) scattering mechanism [9] and provided the index value $A = 1.4$ for sublimation grown epilayer and $A = 1.6$ for CVD grown epilayer. The similar slope values A were found in n- and p-type 4H-SiC samples in temperature range 100–300 K [10–12]. Our data provided $\mu_{\rm h} = 60$ cm^2/(V s) for the CVD grown sample and $\mu_{\rm h} = 40$ cm^2/(V s) for the sublimation grown one at room temperature, that was in good agreement with the Hall data in low doped 4H-SiC epilayers, which provided the hole mobility in range of 60–120 cm^2/(V s) [12, 13]. From Fig. 3 we see that the determined bipolar mobility (diffusion coefficient) values at the same experimental conditions are higher in the CVD grown sample. This can be attributed to the different concentrations of defects.

Carrier scattering mechanisms in 3C-SiC were determined from the magnetoresistance measurements at different temperatures (see Fig. 4). The ionized impurities start to limit the carrier mobility at lower temperatures, but the effect is more pronounced in the epitaxial 3C-SiC layer with respect to 4H-SiC (see Fig. 4). The expected tendencies for scattering by phonons ($\mu_{\rm M} \sim T^{-3/2}$) or by ionized impurities ($\mu_{\rm M} \sim T^{3/2}$) are shown in Fig. 4 by dotted lines [6]. We note that the observed scattering mechanisms of equilibrium carriers by magnetoresistance measurements in 100–300 K temperature interval correlate well with those measured by FWM for highly excited carriers (see Figs. 2, 3, and 4).

The measurements of grating kinetics in highly-

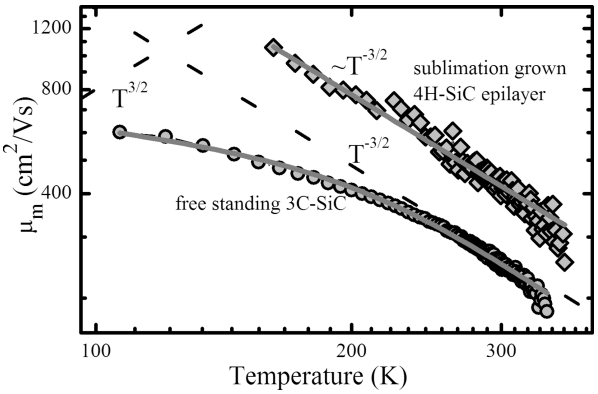

Fig. 4. Magnetoresistant mobility dependence on temperature in free standing 3C-SiC substrate and in n-type 4H-SiC epilayer grown by sublimation technique.

excited free standing 3C-SiC sample at temperatures $T < 50$ K revealed the effect which had been earlier observed in 4H-SiC crystals [14]. The diffraction efficiency kinetics at low temperatures pointed out the contribution of lattice heating to refractive index modulation (see Fig. 5). This effect was earlier observed both in CVD grown 4H-SiC epilayer at temperatures $T < 100$ K as well as in sublimation grown sample at $T < 150$ K [14]. This effect was mainly attributed to nonradiative carrier recombination and lattice heating due to excess quantum energy. In Fig. 5 the grating decay kinetics measured in free standing 3C-SiC sample at different temperatures are presented. The grating decay is single exponential at $T = 100$ K, while at lower temperatures the kinetics become non-exponential and reveal contribution of another mechanism of refractive index modulation. We attribute this effect to refractive index modulation by temperature, previously observed in Si and 4H-SiC [14, 15]. We have found that the contribution of coexisting temperature grating in 3C-SiC is increasing at lower temperature (Fig. 5) and higher excitation energies. At larger grating periods, the contribution of the thermal grating to the total diffraction efficiency is observed at later times (see Fig. 6) or even disappears at $\Lambda = 15.9$ μm, as the carrier grating modulation is less erased by diffusion and persists for a longer time. In the inset of Fig. 6 the kinetics of diffraction efficiency measured in DBP free epilayer at $T = 10$ K and different grating periods are shown. As we see, the lattice heating effect is not present in the sample. Assuming that the lattice heating due to quantum excess energy, nonradiative Auger recombination, and free carrier absorption is similar for both 3C-SiC samples, the more pronounced lattice heating in free standing 3C-SiC layers should be attributed to the additional channels of nonradiative recombination. More detailed analysis of the effect will require an elaborate numerical simulation of carrier dynamics and heating in subnanosecond time domain, using the determined temperature and carrier density dependent mobility and lifetime values in 3C-SiC layers.

5. Summary

The measurements of carrier mobility have been carried out in 3C-SiC and 4H-SiC by using a picosecond four-wave mixing and magnetoresistance techniques. Both techniques confirmed the mechanism of phonon scattering in $T = 100$–300 K range in 4H-SiC. Higher carrier mobility was found in 4H-SiC epitaxial layers grown by standard CVD with respect to 4H-SiC layers grown by sublimation technique, and attributed to higher concentration of defects. Temperature dependences of carrier mobility in 3C-SiC samples confirmed phonon scattering ($T = 100$–300 K), while at lower temperatures ($T < 100$ K) we found ionized impurity governed decrease of carrier mobility. A lattice heating was observed in free standing 3C-SiC and 4H-SiC due to strong impact of nonradiative recombination, and this effect precluded optical studies of carrier dynamics at $T < 50$ K in 3C-SiC and at $T < 100$ K in 4H-SiC.

Acknowledgements

The research was supported by the Lithuanian State Science and Studies Foundation. R. Vasiliauskas acknowledges R. Yakimova, M. Syvajarvi, and G. Ferro for providing samples for the electrical measurements.

References

[1] P. Grivickas, J. Linnros, and V. Grivickas, Mater. Sci. Forum **338–342**, 671–674 (2000).

[2] K. Jarašiūnas, in: *UV Solid-State Light Emitters and Detectors*, NATO Science Series II: Mathematics, Physics and Chemistry, Vol. 144, eds. M.S. Schur and A. Žukauskas (Kluwer Academic Publishers, 2004) pp. 93–109.

[3] K. Neimontas, R. Aleksiejūnas, M. Sūdžius, K. Jarašiūnas, and J.P. Bergman, Mater. Sci. Forum **483–486**, 413–416 (2005).

[4] M. Soueidan and G. Ferro, Adv. Funct. Mater. **16**, 975–978 (2006).

[5] P. Blood and J.W. Orton, *The Electrical Characterization of Semiconductors: Majority Carriers and Electron States* (Philips Research Laboratories, Redhill, Surrey RH15HA, UK, 1992).

[6] I.M. Abdelo-Motaleb and R.Y. Korotkov, J. Appl. Phys. **97**, 093715-1–6 (2005).
[7] S. Juillaguett, C. Balloud, T. Robert, M. Zelinski, and J. Camassel, in: *Abstracts of International Workshop on 3C-SiC Heteroepitaxy*, Grenoble, June 2007, p. 35.
[8] H. Nagasawa, K. Yagi, T. Kawahara, N. Hatta, G. Pensl, W.J. Choyke, T. Yamada, K.M. Itoh, and A. Shoner, in: *Silicon Carbide: Recent Major Advances*, eds. W.J. Choyke, H. Matsunami, and G. Pensl (Springer, Berlin, 2004) pp. 207–228.
[9] J. Singh, *Electronic and Optoelectronic Properties of Semiconductor Structures* (Cambridge University Press, Cambridge, 2003).
[10] T.T. Mnatsakanov, M.E. Levinshtein, L.I. Pomortseva, and S.N. Yurkov, Semicond. Sci. Technol. **17**, 974–977 (2002).
[11] T.T. Mnatsakanov, L.I. Pomortseva, and S.N. Yurkov, Semicond. **35**(4), 394–397 (2001).
[12] H. Matsuura, M. Komeda, S. Kagamihara, H. Iwata, R. Ishihara, T. Hatakeyama, T. Watanabe, K. Kojima, T. Shinohe, and K. Arai, J. Appl. Phys. **96**, 2708–2715 (2004).

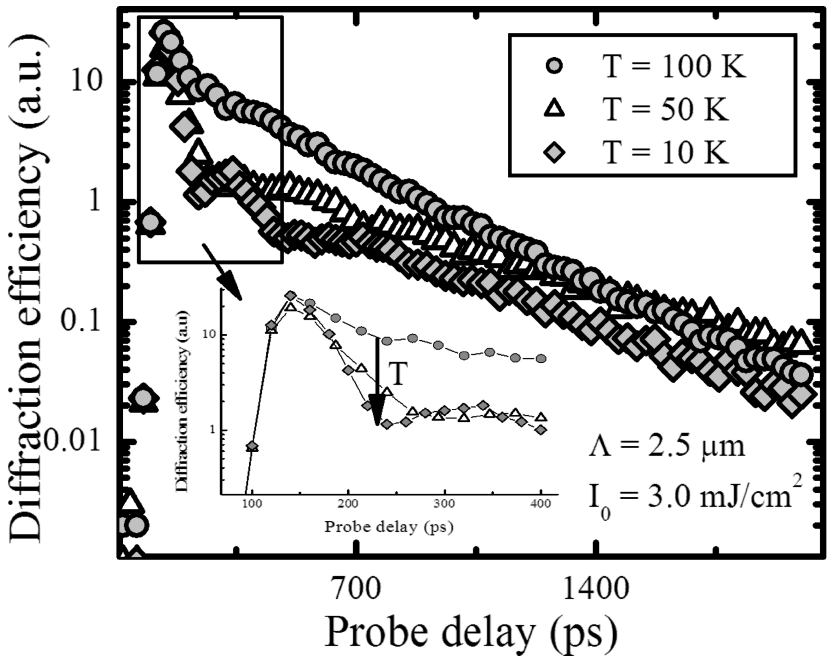

Fig. 5. Kinetics of grating diffraction efficiency measured at different temperatures for the fixed grating period in free standing 3C-SiC. In the inset: grating decay kinetics at first 300 ps after excitation.

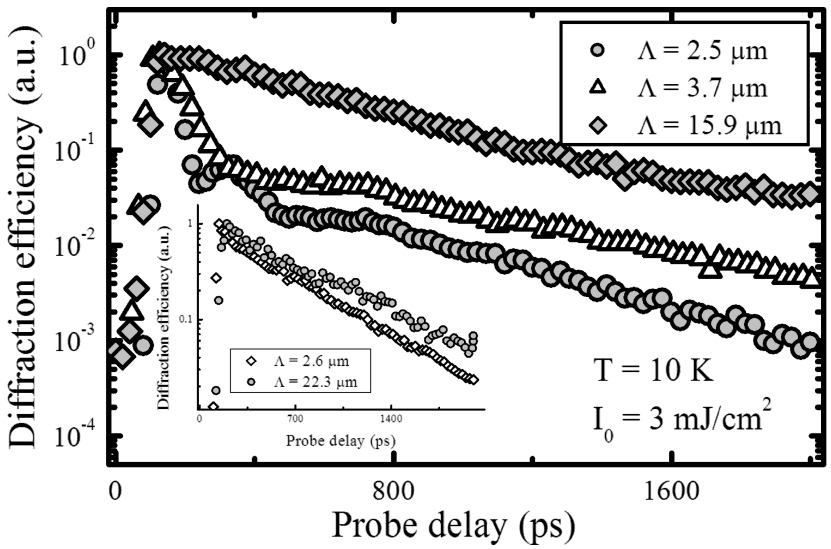

Fig. 6. Kinetics of grating diffraction efficiency measured at different grating periods for the fixed temperature in free standing and DBP free (in the inset) 3C-SiC samples.

[13] W.J. Shatter, H.S. Kong, G.H. Negley, and J.W. Palmour, Inst. Phys. Conf. Ser. **137**, 155–158 (1994).
[14] K. Neimontas, T. Malinauskas, R. Aleksiejūnas, R. Yakimova, and K. Jarašiūnas, Lithuanian J. Phys. **46**, 199–204 (2006).
[15] J. Vaitkus, K. Jarašiūnas, E. Gaubas, L. Jonikas, R. Pranaitis, and L. Subačius, IEEE J. Quantum Electron. **22**, 1298–1306 (1986).

SiC KRISTALŲ TYRIMAI OPTINIAIS IR ELEKTRINIAIS METODAIS

K. Neimontas, R. Vasiliauskas, A. Mekys, J. Storasta, K. Jarašiūnas

Vilniaus universitetas, Vilnius, Lietuva

Santrauka

Keturbangio maišymo bei Holo efekto metodikomis atlikti temperatūriniai nepusiausvirųjų krūvininkų dinamikos matavimai n tipo 4H-SiC ir 3C-SiC epitaksiniuose sluoksniuose bei 3C-SiC kvazitūriniame kristale. Išmatuotos bipolinio krūvininkų judrio (difuzijos koeficiento) priklausomybės 100–300 K temperatūros intervale. Iš abiem metodikomis išmatuotų priklausomybių 4H-SiC epitaksiniuose sluoksniuose ($\mu \sim T^{-3/2}$) nustatyta, kad pagrindinis krūvininkų sklaidos mechanizmas yra sklaida fononais visame matuotos temperatūros intervale (100–300 K). Rastos didesnės difuzijos koeficiento vertės cheminiu garų nusodinimo metodu užaugintame 4H-SiC epitaksiniame sluoksnyje, lyginant su sublimacijos būdu užaugintu bandiniu. Šis skirtumas paaiškinamas skirtingu defektų tankiu abiejuose bandiniuose. Iš išmatuotų krūvininkų judrio temperatūrinių priklausomybių 3C-SiC bandiniuose padaryta išvada, kad sklaida jonizuotomis priemaišomis riboja judrio vertę, kai $T < 100$ K, o esant $T > 100$ K vyrauja sklaida fononais. Judrio vertės mažėjimas didinant žadinančios šviesos energijos tankį (nepusiausvirųjų krūvininkų tankį) kvazitūriniame kristale aiškinamas priemaišų perelektrinimu esant dideliems krūvininkų tankiams. Didesnės judrio vertės (visuose matuotos temperatūros ir žadinančios šviesos energijos tankio intervaluose) kvazitūriniame 3C-SiC lyginant su epitaksiniu sluoksniu rodo geresnes jo elektrines savybes. Nustatyta, kad esant žemai temperatūrai ($T < 100$ K 4H-SiC atveju ir $T < 50$ K 3C-SiC atveju) kristalinės gardelės kaitinimas dėl nespindulinės laisvųjų krūvininkų rekombinacijos ir energijos perviršio, susidarančio žadinant kristalą šviesos kvantu $h\nu > E_{\mathrm{g}}$, sukelia temperatūrinę lūžio rodiklio moduliaciją, kuri turi didelę įtaką difrakcijos efektyvumo kinetikoms, ir dėl to nebegalima tiesiogiai įvertinti nepusiausvirųjų krūvininkų judrio šiuose kristaluose. Reikia pažymėti, kad epitaksiniame 3C-SiC sluoksnyje šis efektas nebuvo stebimas, ir tai rodo mažesnį nespindulinės rekombinacijos kanalų kiekį, lyginant su kvazitūriniu 3C-SiC kristalu.